

The Navier-Stokes Equations in a Rotating Reference Frame and the Shallow Water Model

Michael Wasserstein

July 6, 2021

Abstract

Beginning with the Navier-Stokes equations in an inertial reference frame, we derive the Navier-Stokes equations in a rotating reference frame. We make simplifications to these equations for geophysical fluid dynamics purposes by considering the centrifugal acceleration, Coriolis acceleration, and the acceleration due to changes Earth's rotation rate. Applying our rotating frame equations to a simple atmospheric or oceanic model, the shallow water model, we derive the shallow water equations. Lastly, to verify our interpretations of the shallow water equations, we use Python to conduct numerical simulations of the shallow water model and qualitatively analyze the simulated velocity vector field under varying Coriolis parameters. The velocity vector fields from our simulations confirm our hypothesis about how the field would appear differently under different Coriolis parameters.

Acknowledgements

Fluid dynamics is a fascinating discipline in math, and while I had lots of fun writing this paper, I would not have had the success that I did without the help of several people. Thanks to my Mathematical Methods in Fluid Dynamics classmates for inspiring me, sharing their keen insight, and making me excited to come to class each day. Special thanks go to one anonymous classmate who provided excellent feedback on my draft of this paper. Professor Michael Olinick and Professor Emily Proctor gave me the differential equations and vector calculus tools to be successful in my study of fluid dynamics. Thanks to Jonathan Kemp for assisting me with my computing difficulties when running my numerical simulations. Lastly, thanks to Professor Michaela Kubacki for introducing me to the beauty of fluid dynamics, sharing helpful extremely feedback on my work, and for always being there to answer the array of questions I had.

Table of Contents

Acknowledgements	2
Introduction	4
1 The Navier-Stokes Equations in a Rotating Frame	5
1.1 The Equations in an Inertial Frame	5
1.2 A Vector Rotating in an Inertial Frame	6
1.3 A Rotating Frame	7
1.4 The Equations in a Rotating Frame	10
1.4.1 Centrifugal Acceleration	11
1.4.2 Coriolis Acceleration	13
1.5 Discussion	16
2 The Shallow Water Model	17
2.1 The Model	17
2.2 The Momentum Equation	17
2.3 The Continuity Equation and Boundary Conditions	19
2.4 Discussion	21
3 Simulations of the Shallow Water Model	23
3.1 The Momentum Equation Numerical Method	23
3.2 The Continuity Equation Numerical Method	25
3.3 Setup of the Model	28
3.4 Simulation	29
3.4.1 The Goal of The Simulation	29
3.4.2 The Results	30
3.5 Discussion	33
Conclusion	34
References	35

Introduction

Fluid dynamics is a wide-ranging discipline that has significance in several fields including aeronautics, environmental engineering, geosciences, and biology, among others. When students first encounter fluid dynamics in their studies, they learn the governing equations of fluid flow in an inertial reference frame. When an observer looks at a phenomenon within one frame of reference and the phenomenon is occurring in that same reference frame, these elementary governing equations hold. However, what happens when the observer and the scenario are not in the same reference frame? That is, what if the scenario occurs on a rotating object, while the observer believes that she is in a fixed location and that nothing is rotating? This is what happens on Earth, a planet that rotates 2π radians each day. In this rotating scenario, the governing equations that I alluded to will still hold in most cases. However, for large problems that span thousands of kilometers or multiple days on Earth — like atmospheric or oceanic flow — the governing equations are no longer valid, and we must look at the equations in a rotating reference frame. The governing equations in this rotating form will be the focus of this paper, and they provide the basis for analyzing large-scale geophysical fluid flow problems on Earth.

Three physical principles underpin the governing equations in fluid dynamics: conservation of mass, conservation of momentum, and conservation of energy. By modeling fluid flow in various ways, we can arrive at these governing equations, known as the continuity, momentum, and thermodynamic equations, respectively. As a whole, these equations are the Navier-Stokes equations (NSEs). In their most complete form, the NSEs are rather complex partial differential equations with several terms that describe the internal and external forces that a fluid experiences. However, depending on the properties of the flow, we can make simplifications to these equations. Any analysis of fluid flow problems begins with the governing equations, including the study of fluid dynamics over large scales on Earth. Geophysical fluid dynamics (GFD), the sub-discipline of fluid dynamics that studies these large scale flows, has important implications for weather, climate, and ocean circulation. A basic GFD scenario looks at a “flat” fluid, where the horizontal extent is much larger than the vertical. This problem, known as the shallow water model, can serve as the basis for a more complex understanding of atmospheric-oceanic processes.

In the first section of this paper, we will consider the distinction between rotating and nonrotating reference frames, and we will derive the momentum governing equations in a rotating frame. The focus will be on the momentum equations, since the continuity (mass) and thermodynamic (energy) governing equations have scalar time and spatial dependence, and scalar-dependent equations do not change when we consider the physical principles in a rotating frame. As a result, the continuity and thermodynamic equations are reference frame invariant. Next, we will use the rotating frame equations to examine a simple model of a large-scale fluid, developing the equations for the shallow water model. Lastly, we will use Python to conduct numerical simulations of the shallow water model to examine how the theoretical insights from the derivations relate to what we see numerically.

1 The Navier-Stokes Equations in a Rotating Frame

The derivation presented in this section draws inspiration from similar derivations in geophysical fluid dynamics texts written by Joseph Pedlosky [1], Geoffrey K. Vallis [2], and John Marshall and R. Alan Plumb [3]. Pedlosky’s text, *Geophysical Fluid Dynamics*, is the most mathematically rigorous, thoroughly explaining each step, and while Vallis’ *Atmospheric and Oceanic Fluid Dynamics* also presents a rigorous discussion, the book leaves many details up to the reader. In this section, we will present a complete derivation of the equations, sparing no detail. For a linear algebra focused approach to the derivation, refer to James F. Price’s *A Coriolis Tutorial* [4].

1.1 The Equations in an Inertial Frame

To begin our discussion of the Navier-Stokes equations in a rotating frame of reference, we must first present these equations in an inertial frame. Throughout this paper, we will assume all flows are inviscid, meaning that we can neglect viscosity, mass diffusion, and thermal conductivity. This is convenient in the study of GFD, as we can often treat the atmosphere and oceans as inviscid fluids. Additionally, we will only consider incompressible fluids, since the atmosphere and oceans have nearly constant density. The nonconservation form of the momentum equations for inviscid, incompressible flow, which fluid dynamics texts such as [5] or [6] derive completely, are

$$\frac{\partial u}{\partial t} + u \frac{\partial u}{\partial x} + v \frac{\partial u}{\partial y} + w \frac{\partial u}{\partial z} + \frac{1}{\rho} \frac{\partial p}{\partial x} = f_x, \quad (1a)$$

$$\frac{\partial v}{\partial t} + u \frac{\partial v}{\partial x} + v \frac{\partial v}{\partial y} + w \frac{\partial v}{\partial z} + \frac{1}{\rho} \frac{\partial p}{\partial y} = f_y, \quad (1b)$$

$$\frac{\partial w}{\partial t} + u \frac{\partial w}{\partial x} + v \frac{\partial w}{\partial y} + w \frac{\partial w}{\partial z} + \frac{1}{\rho} \frac{\partial p}{\partial z} + g' = f_z. \quad (1c)$$

Note that we explicitly state the gravitational body force per unit mass, represented by g' , which is the force due to gravitation in Eq. (1c), since it acts in the z -direction and is useful for GFD applications. For now, we will use the notation g' , rather than g , and the reason for this will become clear as we progress through our derivation. Writing these equations in vector notation, we have

$$\frac{D\mathbf{V}}{Dt} + \frac{1}{\rho} \nabla p + g' \hat{\mathbf{z}} = \mathbf{F}, \quad (2)$$

where we made use of the material derivative, $\frac{D}{Dt}$, where

$$\frac{D}{Dt} \equiv \frac{\partial}{\partial t} + \mathbf{V} \cdot \nabla. \quad (3)$$

We now have the inviscid, incompressible momentum equations in an inertial reference frame, and we are ready to derive these equations in a rotating frame.

Lastly, before beginning our derivations, we will present the incompressible continuity equation (which [5] derives) in nonconservation form, given by

$$\nabla \cdot \mathbf{V} = 0. \quad (4)$$

The physical principal behind Eq. (4) is conservation of mass. Because mass is a scalar quantity, it is reference frame invariant, and Eq. (4) does not change in a rotating reference frame. For this reason, we will only derive the momentum equation in a rotating frame.

1.2 A Vector Rotating in an Inertial Frame

First, we consider a vector \mathbf{A} that rotates counterclockwise about an axis of rotation in an inertial reference frame with angular velocity $\boldsymbol{\Omega}$, as shown in Fig. 1.* The angular velocity is the rotation rate of the rotating vector, and it has units of $[\text{s}^{-1}]$ or radians per second. It is the angle $\Delta\theta$ through which the vector rotates in a given amount of time Δt , so that $|\boldsymbol{\Omega}| = \frac{\Delta\theta}{\Delta t}$. As shown in Fig. 1, the angle between \mathbf{A} and the vertical vector about which \mathbf{A} rotates is α , which is a fixed quantity since the distance ℓ between the dashed ellipses is constant. We shall note that we are investigating a fixed and inertial reference frame, and the vector \mathbf{A} rotates within our reference frame.

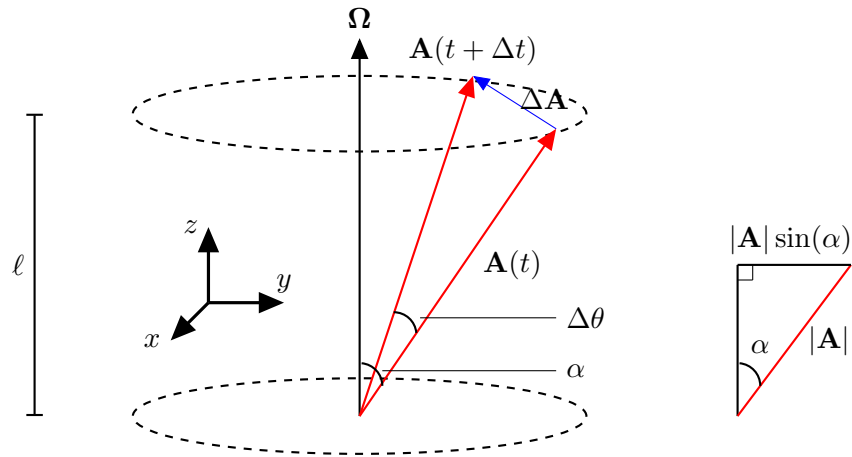


Figure 1: Side view of a rotating vector \mathbf{A} and a cross section of the figure at a given moment in time. The vector rotates counterclockwise with angular velocity $\boldsymbol{\Omega}$, and the angle between \mathbf{A} and the axis of rotation is always α . Note that the distance between the two dashed ellipses is a fixed distance ℓ .

From Fig. 1, we can see that for a small $\Delta\theta = |\boldsymbol{\Omega}|\Delta t$ (implying a small Δt and a small change in \mathbf{A}),

$$\Delta\mathbf{A} = \mathbf{n}|\mathbf{A}|\sin(\alpha)\Delta\theta, \quad (5)$$

where \mathbf{n} is the unit vector in the direction of $\Delta\mathbf{A}$. As the cross section in Fig. 1 shows, $|\mathbf{A}|\sin(\alpha)$ gives the distance from the axis of rotation to the tip of the vectors \mathbf{A} and $\mathbf{A}(t + \Delta t)$ such that if we assume $\Delta\theta$ is small and multiply it by $|\mathbf{A}|\sin(\alpha)$, we get $|\Delta\mathbf{A}|$.

*Although this section is not *crucial* to our derivation of the NSEs in a rotating reference frame, it provides the background that will help us understand how the scenario changes when we consider a rotating reference frame.

Because the tip of \mathbf{A} rotates along one fixed height, $\Delta\mathbf{A}$ is orthogonal to $\mathbf{\Omega}$, such that

$$\mathbf{n} = \frac{\mathbf{\Omega} \times \mathbf{A}}{|\mathbf{\Omega} \times \mathbf{A}|}. \quad (6)$$

If we divide Eq. (5) by Δt and let $\Delta t \rightarrow 0$, $\frac{\Delta\mathbf{A}}{\Delta t}$ becomes instantaneous, given by

$$\frac{d\mathbf{A}}{dt} = |\mathbf{A}| \sin(\alpha) \frac{d\theta}{dt} \frac{\mathbf{\Omega} \times \mathbf{A}}{|\mathbf{\Omega} \times \mathbf{A}|}, \quad (7)$$

where we only take the time derivative of θ since it is the only parameter on the right side that is changing with time. We can now recognize that $|\mathbf{\Omega} \times \mathbf{A}| = |\mathbf{\Omega}| |\mathbf{A}| \sin(\alpha)$, which we substitute into Eq. (7) to arrive at

$$\frac{d\mathbf{A}}{dt} = \mathbf{\Omega} \times \mathbf{A}, \quad (8)$$

where we have made use of the fact that $\frac{d\theta}{dt} = |\mathbf{\Omega}|$. Equation (8) implies that for an observer situated in a reference frame rotating with angular velocity $\mathbf{\Omega}$, the change in \mathbf{A} over an infinitesimal time is

$$\frac{d\mathbf{A}}{dt} = 0, \quad (9)$$

since $\mathbf{\Omega} = 0$ for that observer. Equation (9) tells us that \mathbf{A} is constant for an observer in the rotating reference frame. However, an observer situated inside the inertial frame that we considered in our derivation of Eq. (8) will see the change in \mathbf{A} over an infinitesimal amount of time as the cross product of $\mathbf{\Omega}$ and \mathbf{A} .

1.3 A Rotating Frame

In § 1.2, we examined a vector that rotates in an inertial reference frame. Now, we consider a *rotating* reference frame, in which the vector appears to be fixed in space for an observer situated in that frame. This consideration will serve as the beginning of our derivation of the NSEs in a rotating reference frame, which will ultimately enable us to understand and model large scale flows on Earth. Figure 2 displays a vector \mathbf{A} that rotates counterclockwise about an axis of rotation with angular velocity $\mathbf{\Omega}$. Similarly, vectors $\hat{\mathbf{x}}_{rot}$, $\hat{\mathbf{y}}_{rot}$, and $\hat{\mathbf{z}}_{rot}$ with the subscripts *rot* denote the unit vectors along the x , y , and z axes, respectively, that also rotate counterclockwise about the axis of rotation with angular velocity $\mathbf{\Omega}$. The vectors with the subscript *in* are the unit vectors in the inertial reference frame. For an observer in the inertial frame, these unit vectors are fixed, but for an observer in the rotating reference frame, they appear to rotate clockwise with angular velocity $\mathbf{\Omega}$.

We define

$$\mathbf{A} = A_x \hat{\mathbf{x}}_{rot} + A_y \hat{\mathbf{y}}_{rot} + A_z \hat{\mathbf{z}}_{rot}, \quad (10)$$

where A_x , A_y , and A_z are the components of \mathbf{A} in the x , y , and z directions of the rotating frame, respectively. Because \mathbf{A} appears fixed in the rotating reference frame, the velocity of \mathbf{A} may be given by its time rate of change

$$\left(\frac{d\mathbf{A}}{dt} \right)_{rot} = \frac{dA_x}{dt} \hat{\mathbf{x}}_{rot} + \frac{dA_y}{dt} \hat{\mathbf{y}}_{rot} + \frac{dA_z}{dt} \hat{\mathbf{z}}_{rot}. \quad (11)$$

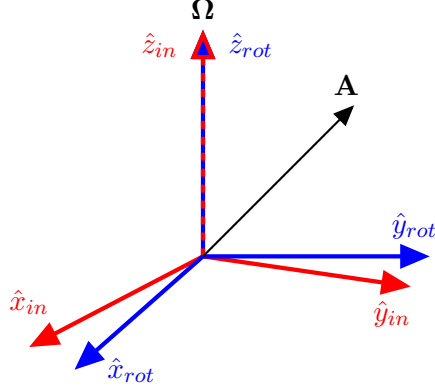


Figure 2: A reference frame rotating counterclockwise with angular velocity Ω . The vector \mathbf{A} rotates counterclockwise about the z-axis with angular velocity Ω , meaning that it is fixed in the rotating frame of reference. The subscripts *rot* denote rotation, while *in* refers to a vector in an inertial reference frame.

For an observer fixed in the inertial frame, $\hat{\mathbf{x}}_{rot}$, $\hat{\mathbf{y}}_{rot}$, and $\hat{\mathbf{z}}_{rot}$ rotate at an angular velocity Ω , and because Ω is perpendicular to the inertial frame,

$$\left(\frac{d\hat{\mathbf{x}}_{rot}}{dt}\right)_{in} = \Omega \times \hat{\mathbf{x}}_{rot}, \quad (12a)$$

$$\left(\frac{d\hat{\mathbf{y}}_{rot}}{dt}\right)_{in} = \Omega \times \hat{\mathbf{y}}_{rot}, \quad (12b)$$

$$\left(\frac{d\hat{\mathbf{z}}_{rot}}{dt}\right)_{in} = \Omega \times \hat{\mathbf{z}}_{rot}. \quad (12c)$$

Now if we take the time derivative of Eq. (10) for an observer in the inertial frame, we have

$$\begin{aligned} \left(\frac{d\mathbf{A}}{dt}\right)_{in} &= \left(\frac{d(A_x\hat{\mathbf{x}}_{rot} + A_y\hat{\mathbf{y}}_{rot} + A_z\hat{\mathbf{z}}_{rot})}{dt}\right)_{in} = \\ &= \left(\frac{d(A_x\hat{\mathbf{x}}_{rot})}{dt}\right)_{in} + \left(\frac{d(A_y\hat{\mathbf{y}}_{rot})}{dt}\right)_{in} + \left(\frac{d(A_z\hat{\mathbf{z}}_{rot})}{dt}\right)_{in}, \end{aligned} \quad (13)$$

and when we apply the product rule to the terms on the right side of Eq. (13), we obtain:

$$\left(\frac{d(A_x\hat{\mathbf{x}}_{rot})}{dt}\right)_{in} = \frac{dA_x}{dt}\hat{\mathbf{x}}_{rot} + A_x\left(\frac{d\hat{\mathbf{x}}_{rot}}{dt}\right)_{in}, \quad (14a)$$

$$\left(\frac{d(A_y\hat{\mathbf{y}}_{rot})}{dt}\right)_{in} = \frac{dA_y}{dt}\hat{\mathbf{y}}_{rot} + A_y\left(\frac{d\hat{\mathbf{y}}_{rot}}{dt}\right)_{in}, \quad (14b)$$

$$\left(\frac{d(A_z\hat{\mathbf{z}}_{rot})}{dt}\right)_{in} = \frac{dA_z}{dt}\hat{\mathbf{z}}_{rot} + A_z\left(\frac{d\hat{\mathbf{z}}_{rot}}{dt}\right)_{in}. \quad (14c)$$

Substituting Eqs. (14a)–(14c) into Eq. (13) and rearranging terms, we obtain

$$\left(\frac{d\mathbf{A}}{dt}\right)_{in} = \frac{dA_x}{dt}\hat{\mathbf{x}}_{rot} + \frac{dA_y}{dt}\hat{\mathbf{y}}_{rot} + \frac{dA_z}{dt}\hat{\mathbf{z}}_{rot} + A_x\left(\frac{d\hat{\mathbf{x}}_{rot}}{dt}\right)_{in} + A_y\left(\frac{d\hat{\mathbf{y}}_{rot}}{dt}\right)_{in} + A_z\left(\frac{d\hat{\mathbf{z}}_{rot}}{dt}\right)_{in}. \quad (15)$$

Now substituting our results from Eq. (11) and Eqs. (12a)–(12c) into Eq. 15, we obtain

$$\left(\frac{d\mathbf{A}}{dt}\right)_{in} = \left(\frac{d\mathbf{A}}{dt}\right)_{rot} + A_x(\boldsymbol{\Omega} \times \hat{\mathbf{x}}_{rot}) + A_y(\boldsymbol{\Omega} \times \hat{\mathbf{y}}_{rot}) + A_z(\boldsymbol{\Omega} \times \hat{\mathbf{z}}_{rot}). \quad (16)$$

Because the cross product has a distributive property and A_x , A_y , and A_z are all scalars, we can rewrite Eq. (16) as

$$\left(\frac{d\mathbf{A}}{dt}\right)_{in} = \left(\frac{d\mathbf{A}}{dt}\right)_{rot} + (\boldsymbol{\Omega} \times A_x\hat{\mathbf{x}}_{rot}) + (\boldsymbol{\Omega} \times A_y\hat{\mathbf{y}}_{rot}) + (\boldsymbol{\Omega} \times A_z\hat{\mathbf{z}}_{rot}). \quad (17)$$

Applying our definition of the vector \mathbf{A} (Eq. (10)) to Eq. (17) we can write the equation in vector form, as

$$\left(\frac{d\mathbf{A}}{dt}\right)_{in} = \left(\frac{d\mathbf{A}}{dt}\right)_{rot} + \boldsymbol{\Omega} \times \mathbf{A}. \quad (18)$$

Equation (18) is crucial in our derivation of the Navier-Stokes equations in a rotating reference frame because it allows us to transform a time derivative of a vector in an inertial frame to one in a rotating frame. To do so, we add a $\boldsymbol{\Omega} \times \mathbf{A}$ to the time derivative of the vector in the rotating frame, as shown in Eq. (18).

Now we consider a velocity vector \mathbf{V} , and we define \mathbf{V} to be the time rate of change of a given position vector \mathbf{r} , so that we may rewrite Eq. (18) as

$$\mathbf{V}_{in} = \mathbf{V}_{rot} + \boldsymbol{\Omega} \times \mathbf{r}, \quad (19)$$

letting \mathbf{r} equal \mathbf{A} and \mathbf{V} equal the time rate of change of \mathbf{A} . If we take the inertial time derivative of Eq. (19) by applying our result from Eq. (18) to Eq. (19) and letting $\mathbf{V}_{in} = \mathbf{A}$, we obtain

$$\begin{aligned} \left(\frac{d\mathbf{V}_{in}}{dt}\right)_{in} &= \left[\left(\frac{d}{dt}\right)_{rot} + \boldsymbol{\Omega} \times\right] (\mathbf{V}_{rot} + \boldsymbol{\Omega} \times \mathbf{r}) \\ &= \left(\frac{d\mathbf{V}_{rot}}{dt}\right)_{rot} + \left(\frac{d(\boldsymbol{\Omega} \times \mathbf{r})}{dt}\right)_{rot} + \boldsymbol{\Omega} \times \mathbf{V}_{rot} + \boldsymbol{\Omega} \times \boldsymbol{\Omega} \times \mathbf{r} \\ &= \left(\frac{d\mathbf{V}_{rot}}{dt}\right)_{rot} + (2\boldsymbol{\Omega} \times \mathbf{V}_{rot}) + (\boldsymbol{\Omega} \times \boldsymbol{\Omega} \times \mathbf{r}) + \mathbf{r} \times \left(\frac{d\boldsymbol{\Omega}}{dt}\right)_{rot}. \end{aligned} \quad (20)$$

To explicitly show how we obtained Eq. (20), we will show the cross-product

$$\left(\frac{d(\boldsymbol{\Omega} \times \mathbf{r})}{dt}\right)_{rot} = \boldsymbol{\Omega} \times \left(\frac{d\mathbf{r}}{dt}\right)_{rot} + \mathbf{r} \times \left(\frac{d\boldsymbol{\Omega}}{dt}\right)_{rot} = \boldsymbol{\Omega} \times \mathbf{V}_{rot} + \mathbf{r} \times \left(\frac{d\boldsymbol{\Omega}}{dt}\right)_{rot}. \quad (21)$$

Note that the second $\boldsymbol{\Omega} \times \mathbf{V}_{rot}$ term on the right side of Eq. (20) comes from the fact that $\left(\frac{d\mathbf{r}}{dt}\right)_{rot} = \mathbf{V}_{rot}$ by definition and $\boldsymbol{\Omega} \times \left(\frac{d\mathbf{r}}{dt}\right)_{rot} = \boldsymbol{\Omega} \times \mathbf{V}_{rot}$ appears in the cross product in Eq. (21).

Remark 1.1. We already explained that the choice of coordinate frame does not affect the continuity equation (Eq. (4)) because we take partial derivatives of a scalar in that equation. To solidify this point, consider an arbitrary scalar B . Because a scalar is a reference frame invariant quantity, we can say

$$\left(\frac{DB}{Dt}\right)_{rot} = \left(\frac{DB}{Dt}\right)_{in}. \quad (22)$$

Equation (22) provides the intuition for why the continuity equation — which involves partial derivatives of mass (a scalar quantity) — does not change in a rotating reference frame.

1.4 The Equations in a Rotating Frame

Section 1.2 set the stage for us to consider the implications of a rotating vector. In § 1.3, we derived the transformation of an inertial frame time derivative of velocity to a rotating frame time velocity derivative, given by

$$\left(\frac{d\mathbf{V}_{in}}{dt}\right)_{in} = \left(\frac{d\mathbf{V}_{rot}}{dt}\right)_{rot} + (2\boldsymbol{\Omega} \times \mathbf{V}_{rot}) + (\boldsymbol{\Omega} \times \boldsymbol{\Omega} \times \mathbf{r}) + \mathbf{r} \times \left(\frac{d\boldsymbol{\Omega}}{dt}\right)_{rot}. \quad (20)$$

The vector form of the Navier-Stokes momentum equation is

$$\frac{D\mathbf{V}}{Dt} + \frac{1}{\rho}\nabla p + g'\hat{\mathbf{z}} = \mathbf{F}. \quad (2)$$

Substituting our our result from Eq. (20) into Eq. (2), our result is the momentum equation in a rotating reference frame:

$$\frac{D\mathbf{V}_{rot}}{Dt} + \frac{1}{\rho}\nabla p + g'\hat{\mathbf{z}} + (2\boldsymbol{\Omega} \times \mathbf{V}_{rot}) + (\boldsymbol{\Omega} \times \boldsymbol{\Omega} \times \mathbf{r}) + \mathbf{r} \times \left(\frac{d\boldsymbol{\Omega}}{dt}\right)_{rot} = \mathbf{F}. \quad (23)$$

In Eq. (23), note that we changed our notation to apply the material derivative to \mathbf{V}_{rot} , since a fluid flow can change with time and space, and this notation follows our notation in Eq. (2). Rearranging Eq. (23) slightly and dropping the subscript *rot* since we will now only consider a rotating reference frame, we arrive at

$$\boxed{\frac{D\mathbf{V}}{Dt} + \frac{1}{\rho}\nabla p + g'\hat{\mathbf{z}} = -(2\boldsymbol{\Omega} \times \mathbf{V}) - (\boldsymbol{\Omega} \times \boldsymbol{\Omega} \times \mathbf{r}) - \left(\frac{d\boldsymbol{\Omega}}{dt} \times \mathbf{r}\right) + \mathbf{F}}, \quad (24)$$

which is the momentum equation in a rotating reference frame.

We should now analyze the momentum equations in our two reference frames more carefully. In the two equations shown in Table 1, we notice three terms added to the

Reference Frame	Momentum Equation
Inertial	$\frac{D\mathbf{V}}{Dt} + \frac{1}{\rho}\nabla p + g'\hat{\mathbf{z}} = \mathbf{F}$
Rotating	$\frac{D\mathbf{V}}{Dt} + \frac{1}{\rho}\nabla p + g'\hat{\mathbf{z}} = -(2\boldsymbol{\Omega} \times \mathbf{V}) - (\boldsymbol{\Omega} \times \boldsymbol{\Omega} \times \mathbf{r}) - \left(\frac{d\boldsymbol{\Omega}}{dt} \times \mathbf{r}\right) + \mathbf{F}$

Table 1: The momentum equation in an inertial and rotating reference frame.

rotating frame equation that are not present in the inertial frame equation: the centrifugal acceleration, $-\boldsymbol{\Omega} \times \boldsymbol{\Omega} \times \mathbf{r}$, the Coriolis acceleration, $-2\boldsymbol{\Omega} \times \mathbf{V}$, and the acceleration due to changes in the rotation rate $\boldsymbol{\Omega}$, given by $-\frac{d\boldsymbol{\Omega}}{dt} \times \mathbf{r}$. Table 2 highlights these three new terms. For oceanic and atmospheric phenomena, $\boldsymbol{\Omega}$ may be treated as a constant so that $\frac{d\boldsymbol{\Omega}}{dt} = 0$, allowing us to neglect the acceleration due to changes in the rotation rate. We shall now examine the other two terms in more depth, beginning with the centrifugal acceleration.

1.4.1 Centrifugal Acceleration

When we consider the momentum equations in a rotating frame, one of the “apparent” forces that arises is the centrifugal force, given by $-\boldsymbol{\Omega} \times \boldsymbol{\Omega} \times \mathbf{r}$. By carefully examining this acceleration and its properties, we will be able to simplify Eq. (24). The centrifugal acceleration points outward from the axis of rotation, and since $\boldsymbol{\Omega}$ is constant it depends solely on how far the fluid is from the center of the Earth. Figure 3 displays the centrifugal acceleration, and this figure will help us analyze its implications. If we let \mathbf{r} be a position vector that rotates counterclockwise about an axis of rotation with angular velocity $\boldsymbol{\Omega}$, then \mathbf{r}_\perp is the vector perpendicular to $\boldsymbol{\Omega}$ and from the axis of rotation to the tip of \mathbf{r} , as shown in Fig. 3. Because $\boldsymbol{\Omega}$ is orthogonal to \mathbf{r}_\perp , $\boldsymbol{\Omega} \times \mathbf{r}_\perp = \boldsymbol{\Omega} \times \mathbf{r}$.

Name	Term
Centrifugal acceleration	$-\boldsymbol{\Omega} \times \boldsymbol{\Omega} \times \mathbf{r}$
Coriolis acceleration	$-2\boldsymbol{\Omega} \times \mathbf{V}$
Acceleration due to changes in $\boldsymbol{\Omega}$	$-\frac{d\boldsymbol{\Omega}}{dt} \times \mathbf{r}$

Table 2: New terms that appear when we consider the momentum equation in a rotating reference frame.

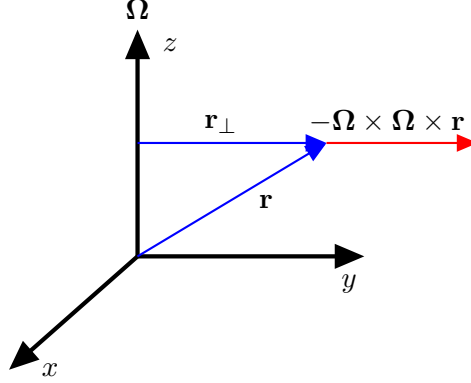


Figure 3: The centrifugal acceleration $-\boldsymbol{\Omega} \times \boldsymbol{\Omega} \times \mathbf{r}$, indicated by the red vector. The vector \mathbf{r} is a position vector in a rotating reference frame with angular velocity $\boldsymbol{\Omega}$, and \mathbf{r}_\perp is the distance vector to \mathbf{r} , perpendicular to the axis of rotation.

Remark 1.2. An important identity in our analysis is the triple product. If we have two vectors \mathbf{A} and \mathbf{B} , we can derive an identity for $\mathbf{A} \times \mathbf{A} \times \mathbf{B}$. It is given by

$$\mathbf{A} \times \mathbf{A} \times \mathbf{B} = (\mathbf{A} \cdot \mathbf{B})\mathbf{A} - (\mathbf{A} \cdot \mathbf{A})\mathbf{B}. \quad (25)$$

We can find a proof of Eq. (25) in any vector calculus textbook, including Susan Jane Colley's *Vector Calculus* ([7]).

Now we can apply the identity given by Eq. (25) to $\boldsymbol{\Omega} \times (\boldsymbol{\Omega} \times \mathbf{r}_\perp)$ to find

$$\boldsymbol{\Omega} \times (\boldsymbol{\Omega} \times \mathbf{r}_\perp) = (\boldsymbol{\Omega} \cdot \mathbf{r}_\perp)\boldsymbol{\Omega} - (\boldsymbol{\Omega} \cdot \boldsymbol{\Omega})\mathbf{r}_\perp. \quad (26)$$

It is clear that $\boldsymbol{\Omega} \cdot \mathbf{r}_\perp = 0$, leaving the centrifugal acceleration as

$$-\boldsymbol{\Omega} \times \boldsymbol{\Omega} \times \mathbf{r} = |\boldsymbol{\Omega}|^2 \mathbf{r}_\perp, \quad (27)$$

where we have replaced $\boldsymbol{\Omega} \times \mathbf{r}_\perp$ with $\boldsymbol{\Omega} \times \mathbf{r}$ since they are equal, and we multiplied Eq. (26) by -1 . The right side of Eq. (27) is just a vector that points entirely in the y -direction in our Fig. 3, and any vector may be written as the gradient of a scalar potential, so we can say

$$-\boldsymbol{\Omega} \times \boldsymbol{\Omega} \times \mathbf{r} = \nabla \left(\frac{|\boldsymbol{\Omega}|^2 \mathbf{r}_\perp^2}{2} \right) = \nabla \phi_c, \quad (28)$$

where $\frac{|\boldsymbol{\Omega}|^2 \mathbf{r}_\perp^2}{2} = \phi_c$. In the middle term of Eq. (28) $|\boldsymbol{\Omega}|$ is simply a constant that we obtained from Eq. (26), and \mathbf{r}_\perp is entirely in the y -direction, so when we take the gradient $\nabla \left(\frac{|\boldsymbol{\Omega}|^2 \mathbf{r}_\perp^2}{2} \right)$, we obtain $(0, |\boldsymbol{\Omega}|^2 \mathbf{r}_\perp, 0)$, which is the centrifugal acceleration, as we can see on the right side of Eq. 27.

Referencing Eq. (24), we can also express the gravity term $g'\hat{\mathbf{z}}$ as a potential, using

$$g'\hat{\mathbf{z}} = \nabla(g'z) = \nabla \phi_{g'}. \quad (29)$$

Defining $\phi_{g'}$ enables us to join potentials in Eq. (24), so that we obtain a potential involving the “measured gravitational potential” g on earth in a rotating frame, where

$$g = \phi_{g'} - \phi_c = g'z - \frac{|\boldsymbol{\Omega}|^2 |\mathbf{r}_\perp|^2}{2}, \quad (30)$$

where the minus sign in front of ϕ_c reflects the fact that we moved the centrifugal equation to the left side of the momentum equation. Note that gravity g' points directly towards the center of the Earth, while the centrifugal acceleration points away from Earth’s rotation axis and perpendicular to it, as shown in Fig. 3. The potential $\phi_{g'}$ reflects Earth’s gravitational pull, while ϕ_c reflects the apparent centrifugal acceleration that appears when we consider the momentum equation in a rotating reference frame.

At last, we can simplify the momentum equation to account only for forces that will “pull” an object to earth when using a rotating reference frame, so that

$$\boxed{\frac{D\mathbf{V}}{Dt} + \frac{1}{\rho} \nabla p + \nabla g = -2\boldsymbol{\Omega} \times \mathbf{V} + \mathbf{F}}, \quad (31)$$

where we have also eliminated the acceleration due to changes in the rotation rate term that we saw in Eq. (24).

1.4.2 Coriolis Acceleration

The Coriolis acceleration — named after French mathematician Gustave Gaspard Coriolis — given by $-2\boldsymbol{\Omega} \times \mathbf{V}$, is the last part of the momentum equation (Eq. (31)) in a rotating frame that we must consider. This acceleration underpins the Coriolis Effect on Earth, which describes the tendency of a moving body to divert its trajectory to the right in the northern hemisphere and to the left in the southern hemisphere. We may treat the Coriolis acceleration as a force per unit mass, which means that this “force” is perpendicular to the velocity \mathbf{V} . Thus, the Coriolis force does *no work* on a moving particle.

Looking more specifically at the anatomy of the Coriolis acceleration, we can see that it involves the negative cross product between the rotation rate $\boldsymbol{\Omega}$ and the velocity of a moving particle \mathbf{V} . This means that the Coriolis acceleration will work to “push” a moving particle towards the right (assuming $\boldsymbol{\Omega}$ is positive), as shown in Fig. 4. If a particle travels with a straight velocity \mathbf{V} , it will turn slightly to the right due to the Coriolis force. This phenomenon has important implications for large-scale atmospheric flow and oceanic circulation on Earth. For instance, if a storm were traveling directly east in the northern hemisphere, it would divert slightly to the south due to the Coriolis force. On the contrary, in the southern hemisphere, Earth’s rotation is clockwise, and the rotation rate vector $\boldsymbol{\Omega}$ points down, causing the Coriolis force to divert moving objects to the left.

We have one additional observation to make about the Coriolis acceleration. Consider a particle located on the surface of the Earth at a latitude φ . We can place the particle at the origin of its own Cartesian coordinate system, denoted by x' , y' , and z' , as shown in Fig. 5. By convention, x' points eastward, y' points to the north, and z' points radially outward from the center of the Earth. Applying trigonometry to the cross-section in Fig. 5, we can

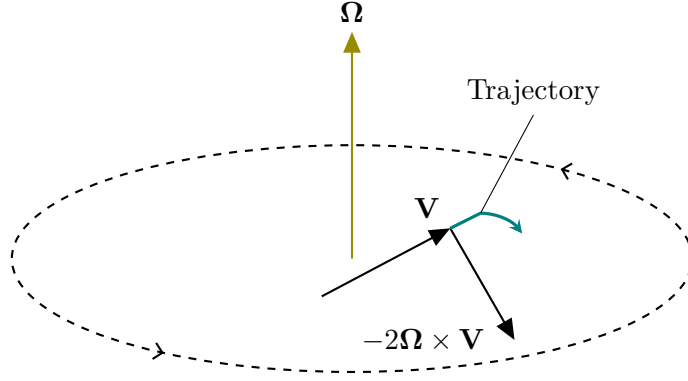


Figure 4: The Coriolis acceleration, which diverts a moving particle with velocity \mathbf{V} to the right. The trajectory that a moving particle would take subject to the Coriolis acceleration is labeled. Note that the rotation is counterclockwise, implying that the system would be in the northern hemisphere on Earth. If the rotation were clockwise, the Coriolis acceleration would divert the particle to the left.

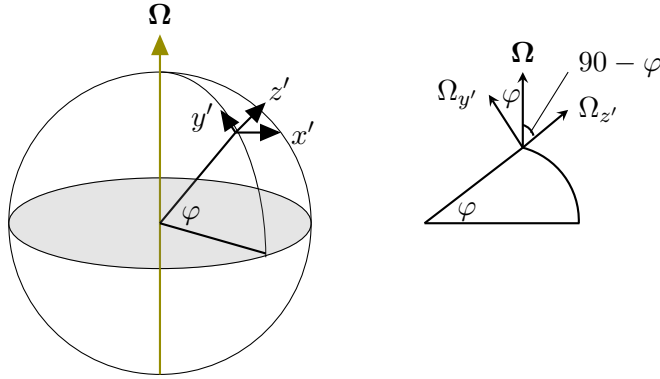


Figure 5: Configuration of a particle located at the origin of a Cartesian coordinate system given by x' , y' , and z' rotating about an axis of rotation with angular velocity Ω and a cross-section of that configuration.

see that $\Omega_{y'} = \Omega \cos(\varphi)$ and $\Omega_{z'} = \Omega \cos(90 - \varphi) = \Omega \sin(\varphi)$, where Ω is the magnitude of Ω and $\Omega_{y'}$ and $\Omega_{z'}$ are the y' and z' components of Ω , respectively. Note that $\Omega_{x'}$ is zero, since Ω points entirely in the vertical direction at the origin of the primed coordinate system (and everywhere). In component form, we can then say $\Omega = (0, \Omega \cos \varphi, \Omega \sin \varphi)$. Once again, the Coriolis acceleration is $-2\Omega \times \mathbf{V}$. If we compute the Coriolis acceleration component wise by taking the cross-product of Ω and \mathbf{V} , we find

$$-2\Omega \times \mathbf{V} = -2(\Omega \cos(\varphi)w - \Omega \sin(\varphi)v, \Omega \sin(\varphi)u, -\Omega \cos(\varphi)u). \quad (32)$$

For the purposes of GFD, the flow in the radial direction (z' , given by w) is *much* smaller than in either horizontal direction (north or east in Fig. 5). As a result, we can manipulate

Eq. (32) by eliminating the term that has w in it. Moreover, since the radial component of the Coriolis acceleration (z') is *much* smaller than the acceleration due to gravity, we can eliminate this term as well, leaving us with

$$-2\boldsymbol{\Omega} \times \mathbf{V} = -2(-\Omega \sin(\varphi)v, \Omega \sin(\varphi)u, 0). \quad (33)$$

We will rewrite Eq. (33) as

$$-2\boldsymbol{\Omega} \times \mathbf{V} = -\mathbf{f} \times \mathbf{V}, \quad (34)$$

where $\mathbf{f} \equiv f\hat{\mathbf{z}}$, and f is the Coriolis parameter given by

$$f \equiv 2\Omega \sin(\varphi). \quad (35)$$

We can now take a deeper look at the Coriolis parameter f . A few things should stand out, which are highlighted in Fig. 6:

1. The Coriolis parameter is positive for $\varphi > 0^\circ$, negative for $\varphi < 0^\circ$, and it is zero for $\varphi = 0^\circ$. In other words, the Coriolis parameter is positive in the northern hemisphere, negative in the southern hemisphere, and zero at the equator.
2. The magnitude of the Coriolis parameter is largest at the poles, and it is smallest at the equator. This implies that the Coriolis acceleration is negligible at latitudes near the equator, but it is most pronounced near the poles.

Our defining of the Coriolis parameter allows us to rewrite the momentum equation in a rotating frame for geophysical purposes. It is:

$$\boxed{\frac{D\mathbf{V}}{Dt} + \frac{1}{\rho}\nabla p + \nabla g + f\hat{\mathbf{z}} \times \mathbf{V} = \mathbf{F}.} \quad (36)$$

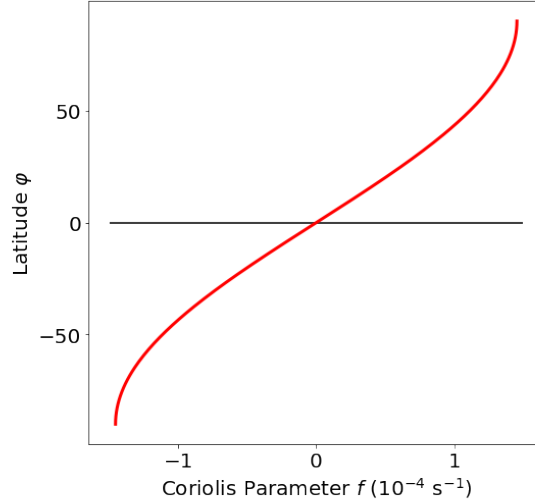


Figure 6: The Coriolis parameter as a function of latitude φ . The plot shows φ on the y -axis and $2\Omega \sin(\varphi)$ on the x -axis for $\Omega = 2\pi$ radians per day.

1.5 Discussion

We will now present the momentum and continuity governing equations of fluid dynamics in a rotating reference frame in the form that is most suitable for geophysical applications for incompressible flows:

$$\boxed{\frac{D\mathbf{V}}{Dt} + \frac{1}{\rho}\nabla p + \nabla g + f\hat{\mathbf{z}} \times \mathbf{V} = \mathbf{F}} \quad (36)$$

$$\nabla \cdot \mathbf{V} = 0 \quad (4)$$

While the continuity equation did not change, the momentum equation differs from its inertial form in two key ways:

1. The potential term contains g , the apparent gravity on Earth that encompasses Earth's gravitation and the centrifugal acceleration.
2. There is the addition of a Coriolis term, which describes the perpendicular “force” that a moving body feels in a rotating system, like Earth.

Equation (36) underpins the study of geophysical fluid dynamics, and it can be applied to simple flow problems to better understand our Earth. In the next section, we will do just that.

2 The Shallow Water Model

We will now apply our work from § 1 to the simplest model in geophysical fluid dynamics, the shallow water model. This model allows us to simplify real-world phenomena in the atmosphere and oceans, which we treat as thin fluids. Real-world modeling of atmospheric flow or global ocean circulation is much more complex than the shallow water model that we will examine, but this model provides the basis for models that are in operational use today.

In this section, we rely most heavily on James C. McWilliams' *Fundamentals of Geophysical Fluid Dynamics* [8], which gives a thorough and mathematically rigorous explanation of the shallow water model. Less detailed but still helpful references are James F. Price's *A Coriolis Tutorial* [1] and *Atmospheric and Oceanic Fluid Dynamics*, by Geoffrey K. Vallis [2]. Lastly, John Marshall and R. Alan Plumb's book, *Atmosphere, Ocean, and Climate Dynamics*, [3] provides a cursory view on the topic, but does not give too much insight. Here, we will derive the continuity equation for the shallow water model from the continuity equation that we already have (Eq. 4). For a derivation of the continuity equation entirely from the physical principles, refer to [2] or [4].

2.1 The Model

In the shallow water model, we assume a constant fluid density and a vertical extent that is much smaller than the horizontal extent (i.e. $H/W \ll 1$, where H is the height of a column in the model and W is the width of the model). Figure 7 shows a simple shallow water model, where H denotes the *average* thickness of fluid, $h(x, y, t)$ is the thickness at a given position and time, η is the surface elevation anomaly at a given position, and B is the bottom elevation of the model at a given position. One important assumption that we will make is that the top surface of the fluid, given by $z = H + \eta$, has time dependence, while the bottom surface $z = B$ has spatial dependence, but it is fixed in time. We define the thickness of the water at a given time and position as

$$\boxed{h(x, y, t) = (H + \eta)(x, y, t) - B(x, y).} \quad (38)$$

2.2 The Momentum Equation

Our first major assumption to make when analyzing the shallow water model is that the flow is entirely horizontal. In other words, the vertical component of velocity \mathbf{V} , given by w , is always zero. As a result, any gradient or divergence in for the shallow water model only takes partial derivatives with respect to x and y (i.e. $\nabla = \left(\frac{\partial}{\partial x}, \frac{\partial}{\partial y}\right)$ for the shallow water model). Thus, in the momentum equation (Eq. (31)), the terms $\frac{D\mathbf{V}}{Dt}$ and $-2\boldsymbol{\Omega} \times \mathbf{V}$ will be zero for the z -component, allowing us to simplify the z -component momentum equation to

$$\frac{\partial p}{\partial z} = -\rho g, \quad (39)$$

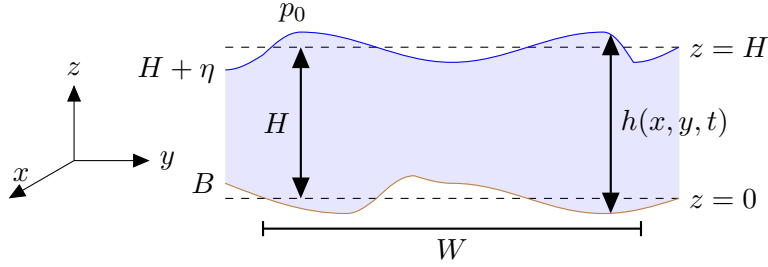


Figure 7: The shallow water model. In this model, H is the mean thickness of the fluid, $h(x, y, t)$ is the thickness at a given point in space and time, W is the width of the model, p_0 is the pressure of the fluid above the fluid in the model, $B(x, y)$ is the height of the bottom surface of the fluid, and $(H + \eta)(x, y, t)$ is the height of the top surface of the fluid.

where we have also eliminated the \mathbf{F} term because there are no vertical external forces in the model. Equation (39) is known as the hydrostatic equation, and integrating it over z , we obtain

$$p(x, y, z, t) = -\rho g z + C, \quad (40)$$

where C is a constant of integration. At the surface of the fluid shown in Fig. 7, we assume a constant pressure p_0 that is equal to the pressure above the fluid, so that

$$p(x, y, H + \eta, t) = p_0. \quad (41)$$

Therefore, we can write Eq. (40) as

$$p(x, y, z, t) = \rho g(H + \eta - z) + p_0. \quad (42)$$

Eq. (42) tells us that at the top of the shallow water model ($z = H + \eta$), the pressure is simply p_0 (as we should expect), and that as we decrease height within a column of the model, the pressure is equal to the pressure at that height in the fluid plus the pressure of the medium above the fluid in the model. From Eq. (42) we can also recognize that the partial derivatives of p in the horizontal are independent of height z . This allows us to write

$$\frac{\partial p}{\partial x} = \rho g \frac{\partial(H + \eta)}{\partial x}, \quad (43a)$$

$$\frac{\partial p}{\partial y} = \rho g \frac{\partial(H + \eta)}{\partial y}, \quad (43b)$$

which implies

$$\frac{1}{\rho} \nabla p = g \nabla(H + \eta). \quad (44)$$

Now substituting into the momentum equation given by Eq. (36), we obtain the momentum equation for the shallow water model in a rotating reference frame, given by

$$\boxed{\frac{D\mathbf{V}}{Dt} + f\hat{\mathbf{z}} \times \mathbf{V} = -g\nabla(H + \eta) + \mathbf{F}.^*} \quad (45)$$

In component form, the momentum equations are

$$\frac{\partial u}{\partial t} + u\frac{\partial u}{\partial x} + v\frac{\partial u}{\partial y} - fv = -g\frac{\partial(H + \eta)}{\partial x} + f_x, \quad (46a)$$

$$\frac{\partial v}{\partial t} + u\frac{\partial v}{\partial x} + v\frac{\partial v}{\partial y} + fu = -g\frac{\partial(H + \eta)}{\partial y} + f_y, \quad (46b)$$

$$\frac{\partial p}{\partial z} = -\rho g. \quad (46c)$$

Note that Eq. (46c) is the differential form of the z-component of the momentum equation for the shallow water, but as we have seen, we can solve this equation to obtain

$$p(x, y, z, t) = \rho g(H + \eta - z) + p_0. \quad (42)$$

We should now discuss Eqs. 46a and 46b more carefully and explain the assumptions we have made in deriving these equations in component form. When applying the material derivative to u and v in Eq. (45), we made note to exclude w ; we do this since w is negligible in the shallow water model. We obtained the Coriolis term in Eqs. 46a and 46b by taking the cross product of $f\hat{\mathbf{z}}$ and u and v , respectively. And the forces per unit mass f_x and f_y are simply the x and y components of \mathbf{F} , respectively, not to be confused with the Coriolis parameter, given by f .

2.3 The Continuity Equation and Boundary Conditions

As we have seen, the continuity equation in the rotating reference frame is

$$\nabla \cdot \mathbf{V} = 0. \quad (4)$$

If we rewrite Eq. (4) in component form and move the x and y derivatives to the right side of the equation, we obtain

$$\frac{\partial w}{\partial z} = -\left(\frac{\partial u}{\partial x} + \frac{\partial v}{\partial y}\right). \quad (47)$$

In the shallow water model, $w \ll u, v$, allowing us to interpret the right side of Eq. (47) as $-\nabla \cdot \mathbf{V}$, so that we can rewrite the equation as

$$\frac{\partial w}{\partial z} = -\nabla \cdot \mathbf{V}. \quad (48)$$

*Note that we have excluded the gravitational potential term ∇g because the term is a function of height z , and z is assumed to be small in the shallow water model. (See Eqs. (29) and (30) for the term ∇g).

Now integrating the right side of Eq. (48) with respect to z , we have

$$\int_B^{H+\eta} -\nabla \cdot \mathbf{V} dz = -(H + \eta - B)\nabla \cdot \mathbf{V} = -h\nabla \cdot \mathbf{V},$$

allowing us to write

$$w(H + \eta) - w(B) = -h\nabla \cdot \mathbf{V}. \quad (49)$$

We now must apply the boundary conditions to the shallow water model. Following the no-slip boundary condition at the bottom surface of the shallow water model (see [5] for more detail on the no-slip condition), we need there to be no normal flow at the surface $z = B$. Consequently,

$$w(x, y, B, t) = \frac{DB}{Dt} = \frac{\partial B}{\partial t} + \mathbf{V} \cdot \nabla B. \quad (50)$$

Equation (50) implies that as the fluid flows at the bottom surface of the shallow water model, its vertical flow w only depends on the shape of the terrain there because we only see partial derivatives of the height B , not the flow, given by \mathbf{V} . For the top of the model, we have

$$w(x, y, H + \eta, t) = \frac{D(H + \eta)}{Dt} = \frac{\partial(H + \eta)}{\partial t} + \mathbf{V} \cdot \nabla(H + \eta) \quad (51)$$

Again, the vertical flow at the top surface is only dependent on the shape of the surface. Substituting our results from Eq. (50) and Eq. (51) into Eq. (49), we obtain

$$w(H + \eta) - w(B) = \frac{\partial(H + \eta)}{\partial t} + \mathbf{V} \cdot \nabla(H + \eta) - \left(\frac{\partial B}{\partial t} + \mathbf{V} \cdot \nabla B \right) = -h\nabla \cdot \mathbf{V}. \quad (52)$$

Simplifying Eq. (52) by applying our definition of the thickness h in the model, given by Eq. (38), we arrive at

$$\frac{\partial h}{\partial t} + \mathbf{V} \cdot \nabla h = -h\nabla \cdot \mathbf{V}, \quad (53)$$

which we can rewrite as

$$\boxed{\frac{Dh}{Dt} + h\nabla \cdot \mathbf{V} = 0}, \quad (54)$$

which is the continuity equation for the shallow water model, where we made use of the material derivative and gradient operator. Note that we included the time derivative of B , given by $\frac{\partial B}{\partial t}$, throughout this derivation. However, given the constraints of the shallow water model described in § 2.1, B is fixed in time, meaning that $\frac{\partial B}{\partial t} = 0$. From Eq. (52), we can then see that

$$\frac{\partial(H + \eta)}{\partial t} - \frac{\partial B}{\partial t} = \frac{\partial(H + \eta)}{\partial t} = \frac{\partial h}{\partial t}, \quad (55)$$

implying that the time derivative of the thickness of the model, given by $\frac{\partial h}{\partial t}$, solely depends on the height of the top surface of the model, given by $H + \eta$.

2.4 Discussion

The system of partial differential equations governing the shallow water model is given by

$$h(x, y, t) = (H + \eta)(x, y, t) - B(x, y), \quad (38)$$

$$\frac{D\mathbf{V}}{Dt} + f\hat{\mathbf{z}} \times \mathbf{V} = -g\nabla(H + \eta) + \mathbf{F}, \quad (45)$$

$$\frac{Dh}{Dt} + h\nabla \cdot \mathbf{V} = 0. \quad (54)$$

We can call Eqs. 38, 45, and 54 the shallow water equations, which are a closed partial differential equation system for \mathbf{V} , h , and η [8]. We shall again note that due to the small nature of the vertical velocity w (so that $\mathbf{V} \approx (u, v, 0)$) in the shallow water model, the material derivative and gradient operators for this model only contain x and y dependence, meaning

$$\frac{D}{Dt} = \frac{\partial}{\partial t} + \mathbf{V} \cdot \nabla = \frac{\partial}{\partial t} + u \frac{\partial}{\partial x} + v \frac{\partial}{\partial y} \quad (57)$$

is the material derivative for the shallow water model.

We can now examine the shallow water equations more carefully and see how they compare to the rotating Navier-Stokes equations. Comparing the shallow water continuity equation (Eq. (54)) to the incompressible continuity equation given by Eq. (4), we see that Eq. (54) includes a material derivative of the thickness h , which was nonexistent in Eq. (4). In Eq. 54 we have a local derivative $\frac{\partial h}{\partial t}$ which describes how the thickness of the model changes over *time*, and we have a convective derivative $\mathbf{V} \cdot \nabla h$ which describes changes in the thickness of the model due to changes in *position* in the horizontal. Equation 54 describes how the mass in the model is conserved in spite of changes in thickness h . Note that the total mass in a given width W may not always be constant, due to possible flow into the model from outside W or flow out of the model, which would result in a changing thickness h . However, the *physical* principle that mass cannot be created or destroyed still holds here.

Our momentum equation, given by Eq. (45), is slightly simpler than the momentum equation in a rotating reference frame (Eq. (36)) because we now only need to solve for a velocity vector field in two directions, the x and y directions. Additionally, the pressure gradient term, given by $\frac{1}{\rho}\nabla p$ in the rotating frame momentum equation, is quite different in the shallow water momentum equation. In the shallow water model, it is $-g\nabla(H + \eta)$. The reason that we see this change is because the pressure in the shallow water model is dependent on the pressure above the model.* For instance, if we assume the fluid in the model is the ocean and the fluid above is the atmosphere, the pressure at given x and y positions will be dependent on the atmospheric pressure. Because w is small in the shallow water model, we do not need to solve for it in the velocity vector field. As a result, the z -component of the shallow water momentum equations is simply the hydrostatic equation, which describes how the pressure in the vertical changes with height. The Coriolis term $f\hat{\mathbf{z}} \times \mathbf{V}$ remains unchanged when we compare the shallow water momentum equation to the

*Recall that the top of the model is at a height $z = H + \eta$.

momentum equation in a rotating reference frame. This invariance makes sense, since the Coriolis acceleration depends on the flow of the fluid relative to the angular velocity, so we should not see any changes under the constraints of the shallow water model.

The shallow water model is an extremely simplified picture of the ocean or the atmosphere, and it serves as the basis for atmospheric and oceanic modeling. While the oceans and atmosphere may be treated as a thin incompressible fluid when we seek to gain a superficial understanding of the flow, we must apply extensions to the model when truly looking to understand or forecast geophysical processes. To do this, we could stack shallow water models on top of each other to generate a layered model, we could account for pressure variations within the ocean and atmosphere, and we could consider shear stresses. The possibilities for extending the shallow water model are endless, but the simplified, incompressible single layer shallow water model develops the foundation for modeling geophysical flows. In the next section, we will model geophysical flows by conducting numerical simulations of the shallow water model.

3 Simulations of the Shallow Water Model

This is the point where we see the payoff of our work in § 1 and 2. We began by deriving the momentum and continuity governing equations of fluid dynamics in a rotating reference frame. We then applied that derivation to a simple geophysical model — the shallow water model. Now, we will conduct numerical simulations of the shallow water model, using open source Python code provided by Jostein Brændshøi, a researcher at the Norwegian Meteorological Institute [9]. By conducting simulations of this nature, we will gain insight into how we model weather, climate, and the oceans, and we will verify our interpretations of the analytical approach to fluid dynamics, which we took in § 1 and 2.

3.1 The Momentum Equation Numerical Method

The source code that we will use makes some important adjustments to the shallow water equations. Specifically, the momentum equations take a linearized form, which allows us to drop the convective term from the momentum equation, eliminating all spatial partial derivatives from Eqs. 46a and 46b. This implies that we will look at a shallow water simulation that assumes Stokes Flow, meaning that the Reynold’s number, a measure of viscosity, is small ($\text{Re} \ll 1$).^{*} Real world examples of Stoke’s flow include the movement of microorganisms or the flow of lava. Additionally, we will assume no external forces, allowing us to remove f_x and f_y from the momentum equations. The code assumes a flat bottom, so that referencing Fig. 7, $z = B = 0$, allowing us to say $h = H + \eta$ at all times. Lastly, in this simulation, we will solve for the *deviation* from the mean height H of the model, meaning we solve for for η , rather than $H + \eta$. Our resulting momentum equations are

$$\frac{\partial u}{\partial t} - fv = -g \frac{\partial(\eta)}{\partial x}, \quad (58a)$$

$$\frac{\partial v}{\partial t} + fu = -g \frac{\partial(\eta)}{\partial y}. \quad (58b)$$

To solve these equations numerically, the code uses a forward-in-time, forward-in-space finite difference method.[†] Specifically, if we want to determine the x -component of velocity, given by u , at a future time $n + 1$ when we know u at a time n , our difference equation (not including the Coriolis acceleration) will be given by

$$\frac{u_m^{n+1} - u_m^n}{\Delta t} = -g \left(\frac{\eta_{m+1}^n - \eta_m^n}{\Delta x} \right), \quad (59)$$

where Δt represents the time step that we use and Δx is the spatial step. Note that in this notation, the superscripts reference a given time, while the subscripts represent a given position in the mesh along the x -domain. Additionally, the x velocity u still has spatial and time dependence, so that

$$u_m^{n+1} = u(x_m, t_n). \quad (60)$$

^{*}In the real world, the atmosphere and oceans do not exhibit Stokes flow.

[†]For a complete discussion of numerical methods and discretization, refer to John D. Anderson’s *Computational Fluid Dynamics* [5].

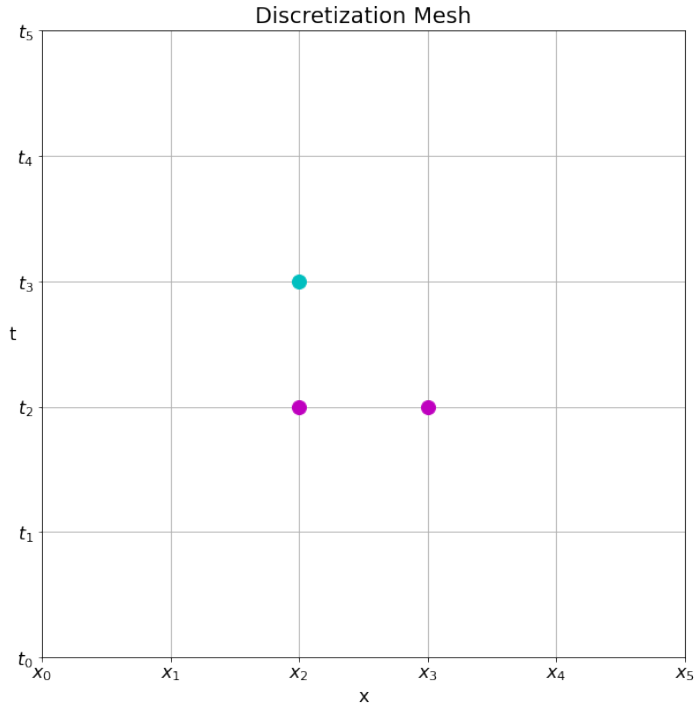


Figure 8: Discretization mesh to solve for a system at a future time, using a forward-in-time, forward-in-space discretization technique. The magenta points denote a known state of the system at t_2 , while the cyan point denotes the location on the grid at which we calculate the state of the system using a finite difference method.

Manipulating Eq. (59), we obtain an explicit solution for the x -component of velocity at a future time $n + 1$, given by

$$u_m^{n+1} = u_m^n - g\Delta t \left(\frac{\eta_{m+1}^n - \eta_m^n}{\Delta x} \right). \quad (61)$$

Note that in Eq. (59) we know all terms on the right side at a time n , so the equation is explicit, and we can solve for u at a time $n + 1$ by plugging in values computed at the previous time step. Figure 8 shows how we can implement the technique used in Eq. (61) to solve for u^{n+1} . The magenta points at (x_3, t_2) and (x_2, t_2) correspond with the known state of the system at $t = t_2$. Referencing Eq. (61), the grid point (x_3, t_2) corresponds with position $m + 1$ and time n , and (x_2, t_2) corresponds with position m and time n . We can plug this known state of the system into the right side of (61), which will give the state of the system at grid point (x_2, t_3) , or the cyan point in Fig. 8, corresponding with position m and time $n + 1$. Note that the grid points displayed in Fig. 8 are not unique, and we could

have created this figure for any three points in our mesh, provided that they are at the points (x_{m+1}, t_n) , (x_{m+1}, t_n) , and (x_m, t_{n+1}) . We can apply a similar technique and logic to the y -component of the momentum equation (Eq. (62)), giving an explicit equation of

$$v_m^{n+1} = v_m^n - g\Delta t \left(\frac{\eta_{m+1}^n - \eta_m^n}{\Delta y} \right). \quad (62)$$

The code to compute u_m^{n+1} and v_m^{n+1} using Eqs. (61) and (62) is

```
1 # Compute u and v at next time step
2 u_np1[:-1, :] = u_n[:-1, :] - g*dt/dx*(eta_n[1:, :] - eta_n[:-1, :])
3 v_np1[:, :-1] = v_n[:, :-1] - g*dt/dy*(eta_n[:, 1:] - eta_n[:, :-1])
```

It is important to note that this code does not contain the crucial Coriolis parameter, which we obtained through our derivation in § 1 and 2. Rather, the arrays that store u and v in the above code are *predictors* of u and v , and we then compute corrected values afterward to include the Coriolis parameter. The code shown below implements this corrector method.

```
1 # Use a corrector method to add coriolis
2 u_np1[:, :] = (u_np1[:, :] - beta_c*u_n[:, :] + alpha*v_n[:, :])/(1 + beta_c)
3 v_np1[:, :] = (v_np1[:, :] - beta_c*v_n[:, :] - alpha*u_n[:, :])/(1 + beta_c)
```

Essentially, after we determine u and v at a future time step, the code uses parameters **beta_c** and **alpha**, which depend on the Coriolis parameter f , in order to correct for the Coriolis effect, modifying the calculated u and v at the future time step. The necessity for implementing this corrector method comes from the nature of the momentum differential equations we seek to solve, given by

$$\frac{\partial u}{\partial t} - fv = -g \frac{\partial(\eta)}{\partial x}, \quad (58a)$$

$$\frac{\partial v}{\partial t} + fu = -g \frac{\partial(\eta)}{\partial y}. \quad (58b)$$

Examining these equations carefully, we see that the x -component equation contains v and the y -component equation contains u . Consequently, the discretization of these equations requires us to incorporate v^{n+1} and u^{n+1} into the x and y -component equations, respectively. To do so, it is necessary to have already calculated v^{n+1} and u^{n+1} ; thus, we use the corrector method for the Coriolis parameter in our discretization.

3.2 The Continuity Equation Numerical Method

The code that we will use solves the continuity equation in its nonlinear form, using forward differences for the time derivatives and an upwind scheme for the spatial components. Additionally, the differential equation that the code solves is slightly different from the one given in Eq. (54) because it solves for η , the deviation from the mean height H , rather

than solving for h . However, in this form of the continuity equation, the conservation of mass principle still holds, but we apply it in a different manner. The equation is given by

$$\frac{\partial \eta}{\partial t} + (H + \eta) \frac{\partial u}{\partial x} + u \frac{\partial \eta}{\partial x} + (H + \eta) \frac{\partial v}{\partial y} + v \frac{\partial \eta}{\partial y} = 0, \quad (64)$$

which we can also write as

$$\frac{\partial \eta}{\partial t} + \frac{\partial((H + \eta)u)}{\partial x} + \frac{\partial((H + \eta)v)}{\partial y} = 0, \quad (65)$$

where we worked backwards from Eq. 64 using the product rule.

To solve Eq. (65) numerically, the code implements an upwind scheme, which models the movement of the flow over time in one direction [5]. Despite having first-order accuracy, an upwind scheme is useful because it only takes finite differences against the direction of the flow, making it less computationally expensive than other discretization methods. In an upwind scheme, we test if the flow in the x and y -direction is positive or negative, and we model the movement of the flow accordingly. In a real-world GFD application, if the wind is moving from the west and we want to know what the wind will be at a future time, an upwind scheme would only look to the west to model the wind. Figure 9 displays an implementation of the upwind scheme. Since the flow is in the positive x -direction, an upwind difference equation would only consider points upstream, which are denoted in blue in the figure.

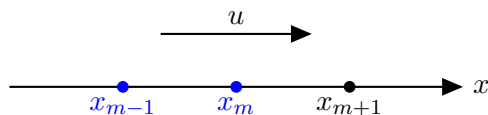


Figure 9: Implementation of an upwind scheme. In this case, u is in the positive x -direction, and we want to solve for u at a point x_m at a future time. To do so, we implement an upwind scheme, considering only where the flow comes from, and disregarding information at x_{m+1} . The blue points indicate points used in the finite difference in the upwind scheme. If the flow were in the negative x -direction, x_m and x_{m+1} would be blue.

Applied to the x -direction in the shallow water model, when the flow is positive ($u > 0$), the difference to determine u at a given grid point m is

$$u_m^{n,+} = \frac{u_{m+1}^{n+1,+}(h_m^{n,+}) - u_m^{n+1,+}(h_{m-1}^{n,+})}{\Delta x}, \quad (66)$$

where the superscripts $+$ denote that we are examining the case where the flow is in the positive x -direction. Recall that in this analysis of the shallow water model, $B = 0$ so $h = H + \eta$, allowing us to use h in Eq. (66). We use our results for u^{n+1} which we calculated in § 3.1, allowing us to find finite differences for u^n . If $u < 0$, we have

$$u_m^{n,-} = \frac{u_{m+1}^{n+1,-}(h_{m+1}^{n,-}) - u_m^{n+1,-}(h_m^{n,-})}{\Delta x}, \quad (67)$$

signifying that the flow is moving in the minus x -direction. For the y -direction, $v_m^{n+1,+}$ and $v_m^{n+1,-}$ will appear the same as Eqs. (66) and (67), respectively, except we replace u with v and Δx with Δy . When we put the results together, the difference equation, given by

$$\eta_m^{n+1} = \eta_m^n - \Delta t \left(\frac{u_m^n}{\Delta x} + \frac{v_m^n}{\Delta y} \right), \quad (68)$$

has u and v terms depend on if the flow is positive or negative. Equation (68) numerically solves Eq. (65) using a forward in time, upward wind scheme numerical method. The code to implement this explicit solution is

```

1     # --- Computing arrays needed for the upwind scheme in the eta equation
      .-----
2     h_e[:-1, :] = np.where(u_np1[:-1, :] > 0, eta_n[:-1, :] + H, eta_n[1:,
      :] + H) # IF true, m-1, m + 1
3     h_e[-1, :] = eta_n[-1, :] + H
4
5     h_w[0, :] = eta_n[0, :] + H
6     h_w[1:, :] = np.where(u_np1[:-1, :] > 0, eta_n[:-1, :] + H, eta_n[1:, :]
      + H)
7
8     h_n[:, :-1] = np.where(v_np1[:, :-1] > 0, eta_n[:, :-1] + H, eta_n[:,
      1:] + H) # depend on sign of v
9     h_n[:, -1] = eta_n[:, -1] + H
10
11    h_s[:, 0] = eta_n[:, 0] + H
12    h_s[:, 1:] = np.where(v_np1[:, :-1] > 0, eta_n[:, :-1] + H, eta_n[:, 1:]
      + H)
13
14    uhwe[0, :] = u_np1[0, :]*h_e[0, :] # u * h
15    uhwe[1:, :] = u_np1[1:, :]*h_e[1:, :] - u_np1[:-1, :]*h_w[1:, :] #
      Difference
16                                # m + 1 upwind h, m, m+1 #m # m, m-1
17    vhns[:, 0] = v_np1[:, 0]*h_n[:, 0]
18    vhns[:, 1:] = v_np1[:, 1:]*h_n[:, 1:] - v_np1[:, :-1]*h_s[:, 1:]
19    # ----- Upwind computations done
      -----
20
21    # ----- Computing eta values at next time step
      -----
22    eta_np1[:, :] = eta_n[:, :] - dt*(uhwe[:, :]/dx + vhns[:, :]/dy) #
      Without source/sink

```

In the above code, line 15 generates u_m^n given in Eq. (66) or (67), depending on if the flow is in the positive or negative x -direction, and line 18 does the same for v_m^n . Line 22 puts everything together, solving Eq. (65). We are now ready to conduct simulations using this model.

3.3 Setup of the Model

Parameter	Value
x -direction Width W_x	1,000 km
y -direction Width W_y	1,000 km
Grid Area	1,000,000 km ² *
Acceleration due to Gravity g	9.81 m/s ²
Mean Fluid Depth H	100 m
Coriolis Parameter f	$1.208 \times 10^{-4} \text{ s}^{-1}$
Number of grid points in x -direction N_x	150
Number of grid points in y -direction N_y	150
Δx	$W_x/(N_x-1)$
Δy	$W_y/(N_y-1)$
Δt	$0.1/\sqrt{(gH)}$
Number of time steps in simulation	3000

Table 3: Parameters for the numerical simulation.

Like most numerical methods for solving partial differential equations, we will utilize a grid with fixed widths, where h , u , and v can vary with time. Table 3 shows several parameters that we use for this model. To initialize the height deviation from H , given by η , we can define a mesh of values for η that has some randomness at each grid point. The code to do this is

```

1 # Initial condition for eta.
2 eta_n[:, :] = np.sin(4*np.pi*X/L_y) + np.sin(4*np.pi*Y/L_y)

```

which generates an initialized height deviation η , as shown in Fig. 10. Notice that we intentionally assign some locations to have surface elevation anomalies $\eta > 0$, while other locations have surface anomalies $\eta < 0$. This initialization is not realistic for atmospheric or oceanic phenomenon, but it will be interesting to analyze when we conduct our simulations, since the continuity equation (Eq. (65)) shows that the velocity vector field is highly dependent on the surface elevation η .

Because the initialized η varies throughout the mesh, we can initialize u and v at 0 m/s, so that the initial movement occurs entirely due to the continuity equation (Eq. (65)). This movement will cause u and v to change, and cause the velocity vector field to change at each time step. By choosing a time step Δt of $0.1/\sqrt{(gH)}$, the simulation that we will run is stable under the Courant-Friedrichs-Lewy stability condition, given by

$$\Delta t \leq \frac{\Delta x}{\sqrt{(gH)}} \quad (69)$$

*For reference, the total area of the Mediterranean Sea is approximately 2,510,000 km², so our domain is about half the size of the Mediterranean Sea.

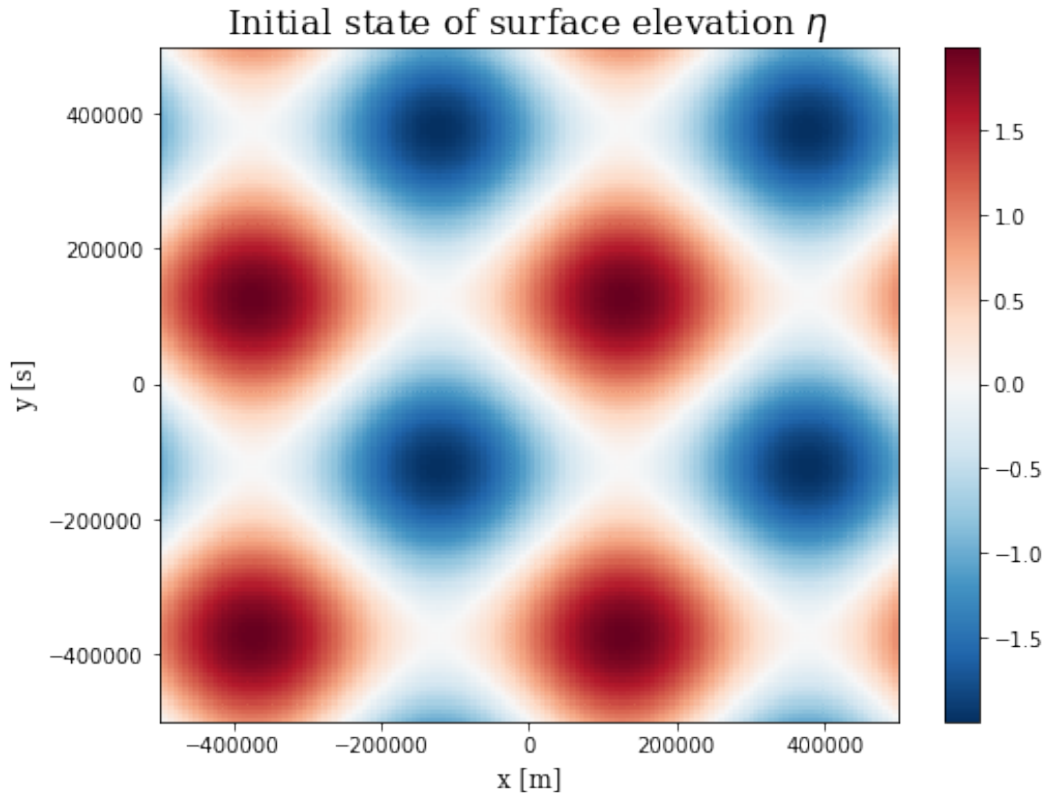


Figure 10: Initialization of the surface elevation η in the shallow water model for our simulations. Red colors denote a surface height above the mean height H , and blue colors denote a surface below H .

for the x -direction [10]. The same condition holds in the y -direction, except we replace Δx with Δy .

3.4 Simulation

We are now ready to complete our simulation of the shallow water model. As previously discussed, we will use the initialization shown in Fig. 10 and an initial velocity vector field of $\mathbf{V} = \vec{0}$.

3.4.1 The Goal of The Simulation

In our simulations of the shallow water model, we will examine the impact of the Coriolis acceleration at different latitudes. By choosing a fixed Coriolis parameter for different simulations of the shallow water model and visualizing the velocity vector field \mathbf{V} for the different simulations, we will be able to qualitatively describe the impact of the Coriolis acceleration on the flow. With 3,000 total time steps in our simulation, we will numerically simulate 17.86 hours of the shallow water model. We will look at snapshots of the velocity

vector field at time steps 1,000 and 2,000, which correspond with hours 5.95 and 11.9 of the simulation, respectively. Table 4 displays the latitudes and Coriolis parameters for each simulation of the shallow water model that we will run. Because the Coriolis acceleration is given by $f\hat{\mathbf{z}} \times \mathbf{V}$, we should expect to see the largest diversions in the velocity vector field due to the Coriolis acceleration at the highest latitudes, which are in simulations 3 and 4.

Simulation	Latitude φ ($^\circ$)	Coriolis parameter f (10^{-4} s^{-1})
1	0	0
2	30	0.727
3	60	1.26
4	90	1.454

Table 4: Latitudes and Coriolis parameters for each simulation.

3.4.2 The Results

As mentioned in § 2, this analysis is strictly qualitative, and we will examine how the velocity vector field at a given time within the simulations changed as we changed the latitude of the simulation (along with the Coriolis parameter). Figures 11 and 12 display the velocity vector field \mathbf{V} at 5.95 and 11.9 hours into the simulation, respectively. Examining the figures, we can see that at all latitudes, there appear to be “sources” and “sinks”, or locations from which the flow travels to or leaves, respectively. Since we assumed that the density of the fluid is constant for this model, there is no pressure gradient responsible for these sources and sinks. Rather, the conservation of mass principle (Eq. (65)) causes these sources and sinks in the velocity vector field. Because our initialization of the mean height deviation η (shown in Fig. 10) had peaks and valleys, the flow – which was entirely due to changes in η – takes on a “wavy” trajectory, with the flow approaching a specific location at times and leaving at other times.

While the source and sink pattern unites the simulations at different latitudes, we can see a clear distinction in the *trajectory* of the flow as we alter the latitude. As hypothesized, when we increase the latitude at which we conducted the simulation, the curvature in \mathbf{V} increases, as shown in Figs. 11 and 12. We can attribute this finding entirely to the Coriolis effect, which was the only parameter that we modified in the simulations. For example, Fig. 12a, which shows \mathbf{V} at the equator, has a very vertically and horizontally oriented vector field, with no true curvature in the flow. However, when we examine Figs. 12c and 12d, which increase the latitude to $\varphi = 60^\circ$ and $\varphi = 90^\circ$, respectively, we notice that the vector field diverts significantly from this vertically oriented structure. Moreover, this “diversion” is to the right, which we should expect given that the Coriolis parameter is positive, meaning that the rotation is counterclockwise. Thus, the velocity vector fields verify our analytical interpretation of the Coriolis effect from § 1.4.2.

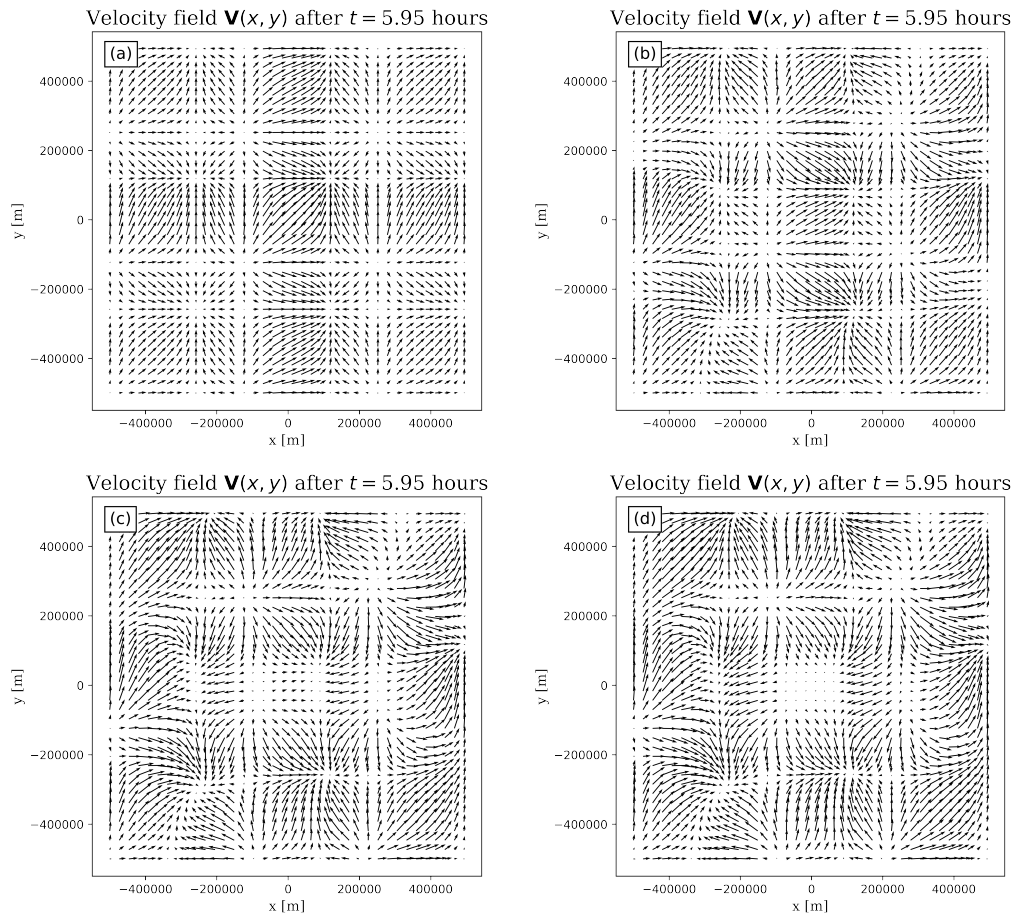


Figure 11: The velocity field at 5.95 hours into the simulation for latitudes (a) $\varphi = 0^\circ$, (b) $\varphi = 30^\circ$, (c) $\varphi = 60^\circ$, and (d) $\varphi = 90^\circ$.

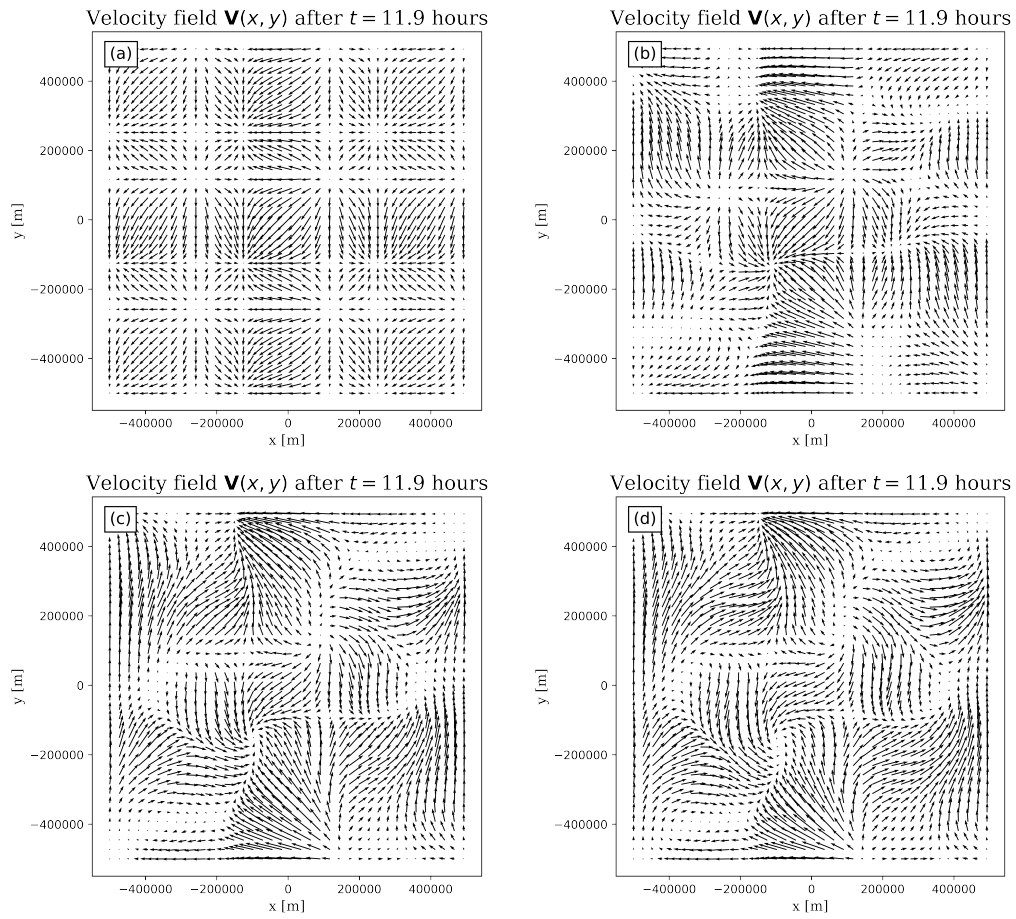


Figure 12: The velocity field at 11.9 hours into the simulation for latitudes (a) $\varphi = 0^\circ$, (b) $\varphi = 30^\circ$, (c) $\varphi = 60^\circ$, and (d) $\varphi = 90^\circ$.

3.5 Discussion

Our work in § 1 and 2 planted the seeds for conducting numerical simulations in § 3. When we derived the NSEs in a rotating reference frame, we saw that a few new terms appeared. The term of interest for geophysical purposes was $-2\boldsymbol{\Omega} \times \mathbf{V}$, the Coriolis acceleration. Because this term was on the right side of the momentum equation and we want to solve that equation for \mathbf{V} , which is a partial derivative on the left side of the equation, we concluded that the Coriolis acceleration would divert a flow to the right, and it would do so to a greater extent at higher latitudes, where the magnitude of $\boldsymbol{\Omega}$ is greater. Our results of the simulations we conducted in this section numerically verify what we previously derived, showing an enhanced curvature and diversion in \mathbf{V} as the latitude increased.

Conclusion

In fluid dynamics, there are three dimensions: the experimental dimension, the theoretical dimension, and the computational dimension. In this paper, we bridged the gap between two of these dimensions – the theoretical and the computational. We first noted a key problem in the inertial reference frame Navier-Stokes equations. While they provide strong detail and insight when analyzing flows on small spatial and time scales, when analyzing flows on larger scales, like Earth’s oceans or the atmosphere, the inertial frame equations do not suffice. We tackled this problem by noting that Earth is a rotating body, so we derived the Navier-Stokes equations in a rotating reference frame. We uncovered new terms in the equations, such as the Coriolis term, which describes the tendency of a moving body to divert its trajectory. This term is crucial when considering tropical storm formation or oceanic circulation, and it is non-existent in the inertial frame Navier-Stokes equations. We applied our derivation to the shallow water model, obtaining the shallow water equations. Lastly, we connected our theoretical study to a computational one, by conducting numerical simulations of the shallow water model at different latitudes. In geophysical fluid dynamics, it is nearly impossible to consider the experimental dimension of fluid dynamics; Earth’s atmosphere and oceans are so large and operate on such a long time scale that taking velocity and density measurements at all locations within these fluids is not practical.

This work is important because it serves as the basis for understanding the complex and dynamic processes in Earth’s oceans and atmospheres. Why does a tropical storm spin counterclockwise in the northern hemisphere and clockwise in the southern hemisphere but is unable to form at the equator? That is due to the *Coriolis effect*. Why is Earth’s net acceleration due to gravity equal to $g = 9.81 \text{ m/s}^2$? That is in part due to gravitation, but it is also due to the *centrifugal acceleration*. Both the Coriolis term and the centrifugal term arise in the NSEs only when we consider the equations in a rotating reference frame. Because we made this consideration, we can better understand the processes that underpin large-scale flows on Earth.

To extend the work in this paper, we could analyze the velocity vector field generated in our numerical simulations with a more quantitative approach. For instance, we could look at velocity vectors at unique points in our mesh for each of our four simulations and devise a mathematical formula to compare the differences in velocity vectors at given times. We would then have a rigorous understanding of how the Coriolis acceleration impacts the flow. To continue the work from § 2, we could develop a multi-layer shallow water model, in which the characteristics of each layer are different (e.g. differing densities). Generating the equations to govern this model would paint a truer picture of the oceans and atmosphere, as layers within the ocean and atmosphere have different densities. After generating the equations for this multi-layer shallow model, we could again analyze them numerically to see if trends that we saw with a single layer arise when we consider multiple layers. This work is a foundation for diving deeper and exploring the fascinating nature of large-scale fluids on Earth.

Honor Code Pledge:

I have neither given nor received any unauthorized aide on this assignment.

Michael Wasserstein

References

- [1] Joseph Pedlosky. *Geophysical Fluid Dynamics*. Springer-Verlag, 1987.
- [2] Geoffrey K. Vallis. *Atmospheric and Oceanic Fluid Dynamics*. Cambridge University Press, 2017.
- [3] John Marshall and R. Alan Plumb. *Atmosphere, Ocean, and Climate Dynamics: An Introductory Text*. Elsevier Academic Press, 2008.
- [4] James F. Price. *A Coriolis Tutorial*. Woods Hole Oceanographic Institution, 2016.
- [5] John D. Anderson Jr. *Computational Fluid Dynamics: The Basics with Applications*. McGraw Hill, (India) edition, 1995.
- [6] G.K. Batchelor. *An Introduction to Fluid Dynamics*. Cambridge University Press, 1967.
- [7] Susan Jane Colley. *Vector Calculus*. Pearson Education, 4 edition, 2012.
- [8] James C. McWilliams. *Fundamentals of Geophysical Fluid Dynamics*. Cambridge University Press, 2006.
- [9] Jostein Brændshøi. shallow-water, 2019. Accessed 4/12/2021. Available at <https://github.com/jostbr/shallow-water>.
- [10] Erwan Deriaz and Pierre Haldenwang. “Von Neumann Stability Analysis of the Upwind Finite Difference Schemes”. 2013.